Band-Limited Signal Reconstruction from Irregular Samples with Variable Apertures[*]

David G. Long and Reinhard O. W. Franz
Brigham Young University

November 20, 2015

Abstract

Sampling plays a critical role in remote sensing and signal analysis. In conventional sampling theory, the signal is sampled at a uniform rate at a minimum of twice the signal bandwidth. Sampling with an aperture function requires a fixed aperture function, which can be removed by deconvolution after signal reconstruction. However, in some cases the signal samples are available only at irregular positions and different samples use different aperture functions.

Here we explore the theory of finite-length signal reconstruction with irregular samples and variable apertures in one and two dimensions is considered. We concentrate on discrete sampling and reconstruction.

In the one-dimensional case, a band-limited discrete signal can be *exactly* reconstructed from a finite number of arbitrarily spaced samples with few restrictions on the aperture functions, which can vary between samples.

Exact reconstruction in the two-dimensional case requires the sampling location matrix be invertable, and is not always possible. Variable aperture functions, while complicating the process, can enable reconstruction for a broader range of sample locations. Note that two-dimensional reconstruction from general cubic lattice samplings, which include uniform sampling, are always fully invertable in the ideal aperture case.

We consider a number of practical issues and provide some numerical examples based on simulated special sensor microwave imager (SSM/I) radiometer measurements which have variable apertures. We note that variable aperture reconstruction has application in a variety of remote sensing and other signal processing problems.

1 Introduction

In a typical remote sensing application, observations (measurements) are samples of an aperture-filtered signal, typically a distributed geophysical quantity such as surface brightness temperature. The aperture results from spatial filtering characteristics of the antenna,

---

optics, and/or signal processing used in the signal sampling. Signal sampling may involve a combination of platform movement, scanning, and pulsed operation, among others. The signal and sampling are frequently two-dimensional. From the set of samples we desire to reconstruct the original signal over the sampling area.

Reconstruction of a band-limited signal from uniformly spaced samples is a well-understood problem treated in standard signal processing textbooks (e.g., [1]): given uniformly spaced samples of the signal, the original band-limited signal can be exactly reconstructed from the samples by sinc interpolation[1] so long as the signal is sampled at twice the highest frequency of the signal, i.e. as long as the sampling meets the Nyquist criterion. Uniform spacing of the samples is also known as "regular sampling". We note that this traditional band-limited reconstruction relies on infinite samples, which cannot be practically collected. We thus need to consider more general reconstruction techniques [2]. Approximate solutions based on oversampling and filtering or interpolation are commonly used[2] Alternately, we can use the periodic extension method explored in the following.

When the signal is sampled with a fixed aperture function[3], the original signal can be recovered from the samples by deconvolution of the aperture function and an intermediate signal resulting from reconstruction from the samples assuming no aperture function[4]. So long as the spectrum of the aperture function has no nulls in the signal bandwidth, the original signal can be completely recovered. Otherwise, there may some loss of information.

In some remote sensing applications, only a finite number of measurements are available and the observations (samples) are not uniformly spaced due to the sensor measurement geometry or platform motion, resulting in irregular (non-uniformly spaced) sampling. Furthermore, the effective aperture may be different for each of the observations, a condition termed "variable aperture" sampling. A number of techniques have been published for signal reconstruction from irregular, arbitrarily spaced samples, e.g. [2, 5, 6, 7, 8, 9] and references therein; however, the general solution to the problem of signal reconstruction from irregular sampling with variable aperture functions has only been recently developed [10], and the limitations of reconstructability for two dimensions have not been fully addressed.

To make this earlier work more accessible we use a tutorial approach to discuss the problem of band-limited signal reconstruction from irregular samples for variable and fixed apertures and present a general discrete signal solution in one and two dimensions. The discrete signal method is chosen since in practice the signals of interest are defined only over a bounded domain and only a limited number of samples are available. This report includes new contributions such as a discussion of practical considerations, a presentation of the sampling limitations in two-dimensional reconstruction from the irregular sampling, an empirical analysis of the ratio of sample density and bandwidht, and a derivation of the general matrix formulation for irregular sampling with variable apertures. To illustrate the technique simulation results are presented for a realistic sensor.

---

[1]Sinc interpolation is equivalent to low-pass filtering of a zeroth-order hold signal.

[2]An example is interferometric SAR data analysis for which window-based interpolation schemes have been developed [3, 4].

[3]An aperture function is also termed a point-spread function, a spatial response function, or an impulse response function.

[4]This is equivalent to assuming an ideal delta function aperture function.

This article is organized as follows: after background and discussion, using a matrix approach we show that a band-limited one-dimensional signal can be reconstructed from arbitrarily located samples. We then extend the derivation to the case of variable apertures. We then consider two-dimensional signals, which requires some constraints on the locations of the irregular samples to ensure full reconstruction. An illustrative example is provided demonstrating the utility of the technique in remote sensing based on reconstruction of brightness temperature images from spaceborne radiometer data.

1.1 Background

In this section we discuss classic reconstruction theory for continuous-time signals, the connection between continuous-time and discrete-time signals, and the reconstruction of discrete-time signals from ideal and aperture-filtered, uniformly-space samples.

Consider two fundamental ideas in signal analysis: (1) the periodicity assumption implied by discrete sampling of a band-limited, finite-length signal and (2) discrete subsampling. We note that all practical signals are bounded.

When teaching introductory signal processing it is common to assume infinite length, continuous signals (e.g., $f(t) = \sin t$). In analyzing ideal one-dimensional signal reconstruction from samples, a continuous band-limited signal $f(t)$ is uniformly sampled at an interval of T with an infinite number of samples. The ideally sampled signal is written as $f[n] = f(nT)$ where $f[n]$ is a discrete-time signal with n an integer. Assuming that $1/T$ is greater than the twice the highest frequency present in $f(t)$ (often called the "Nyquist sample rate"), the Shannon-Wittaker-Kotel'nikov sampling theorem (see [1]) assures us that $f(t)$ can be reconstructed from $f[n]$ using

$$f(t) = \sum_{n=-\infty}^{\infty} f[n]\mathrm{sinc}((t - nT)/T) \tag{1}$$

where $\mathrm{sinc}(x) = \sin(\pi x)/\pi x$.

In practice, however, we can only observe a signal over a finite domain with a finite number of samples. Unless the form of the underlying signal is known analytically, an arbitrary signal cannot generally be fully reconstructed from only a finite number of samples. We recall that when sampling a signal there is an *implicit assumption that the signal is band-limited*; otherwise, aliasing and loss of signal information occurs in representing the signal from its samples [1].

Note that only periodic signals can be band-limited. A finite-length signal can be made periodic by extension. If we assume that the signal being sampled is periodic, and that the signal samples correspond to one or more periods of the periodic signal, we can, in practice, consistently assume that the signal is band-limited. This enables the (periodic, band-limited) signal to be exactly reconstructed from the signal. This suggests that even if underlying signal is not believed to periodic, the act of sampling and reconstruction implicitly requires that we treat the signal as periodic and band-limited in order for the idea of accurate reconstruction from samples to make sense.

Recalling that a finite-length signal can be made periodic by extension, we note that in order for a signal to be consistently represented by a finite number of samples and be

simultaneously band-limited, we must assume the signal to be periodic. In effect, finite sampling and reconstruction implicitly requires that we treat the signal as both periodic and band-limited in order to consistently interpret sampling and reconstruction. We note that a bounded, continuous, band-limited, periodic signal can always be exactly represented by a discrete-time signal [1, 10].

With these preliminaries, we observe that the sampling of a band-limited, continuous signal can be viewed as equivalent to subsampling a discrete-time signal corresponding to the original signal. To explore this for a one-dimensional signal, denote the signal of interest by $f(t)$. Suppose there are R samples of $f(t)$ available at the arbitrary sample points $t = t_j$ for $j = \{1...R\}$. Real-world considerations suggest that the spacings of the sample points have a rational relationship. Thus, t_j can be written as

$$t_j = n_j T + T_0 \tag{2}$$

where n_j is an integer, T_0 is a real constant, and T is some interval for which Eq. 2 holds for all j. In general, there are an infinite number of possible T values.[5] We prefer to choose the largest T subject to $1/T > 2B$, where B is the highest frequency present in the band-limited $f(t)$. This T is hereafter referred to as the high-rate sample interval (HSI).

Based on the earlier discussion, since the signal $f(t)$ is band-limited, it can be exactly represented by its discrete-time counterpart $f[n] = f(nT)$ where T is the HSI. Thus, for practical signal reconstruction, we need only reconstruct $f[n]$ from the samples $f[n_j]$. The signal $f(t)$ can be reconstructed from $f[n]$ using Eq. 1 where the infinite sum in Eq. 1 is computed modulo the period so that only one period of the values of $f[n]$ are required.

Thus the sampling of the continuous signal $f(t)$ is equivalent to the discrete sampling of the discrete signal $f[n]$. The available samples extend over the finite domain defined by NT where T is the HSI and NT is the (assumed) signal period. The period count N may be larger than $\max(n_j) - \min(n_j)$, but if smaller, the indices n_j are mapped to $n \in \{0, ..., N-1\}$. Without information about the signal structure, selection of N in practice can be arbitrary and requires engineering judgment.

The discrete Fourier transform (DFT) $F[k]$ of $f[n]$ can be written as

$$F[k] = \sum_{j=0}^{N-1} f[j] W_N^{kj} \tag{3}$$

where $W_N^{kj} = e^{-i2\pi kj/N}$ and $i = \sqrt{-1}$ [1]. Since $f[n]$ is band-limited to B, $F[k] = 0$ for all $|k| > M$ where $M \le NB/2T$, and the discrete signal $f[n]$ is termed M-band-limited. Note that $F(k)$ approximates the continuous Fourier transform $F(\omega)$ of the underlying continuous $f(t)$ for $\omega < \pi M/NT$ [1].

In the one-dimensional case, the M-band-limited discrete signal $f[n]$ can be perfectly reconstructed from the irregular samples $f[n_j]$ for arbitrary n_j, so long as the $R \ge 2M + 1$ samples $n_j \bmod N$ are distinct [8]. Additional samples can reduce the effects of noise in

---

[5]This is readily seen by noting that if a particular value of T satisfies Eq. 2 for all j, the value d where $T = md$ for an arbitrary integer $m > 0$ also satisfies Eq. 2.

noisy processes [6, 5]. Efficient numerical algorithms for irregular reconstruction have been developed [6].

As discussed later, unlike one-dimensional reconstruction, two-dimensional reconstruction is not always possible for arbitrarily located samples. Accurate two-dimensional reconstruction imposes restrictions on the sample locations.

The sampling discussed so far assumes an ideal aperture function where the observation of the signal $f[n]$ at n_j is $f[n_j]$. Practical aperture functions result in observation values that are locally averaged and weighted values of the signal. Local averages smaller than the maximum sample spacing are treated by [11]; however, as discussed below, larger apertures can be used. In general the observation values can be modeled as ideal samples of the aperture-filtered signal. For example, in one dimension using the discrete signal model with the aperture function $v[n]$, the observation sample is $g[n_j]$ where g is the aperture-filtered signal given by $g[n] = v[n]*f[n]$ where $*$ denotes discrete convolution. For the fixed-aperture case, the samples can be first used to reconstruct $g[n]$ from the observations, then signal deconvolution techniques can be used to compute $f[n]$ from $g[n]$. So long as the aperture spectrum does not have any nulls over the bandwidth of the signal spectrum, the signal can be reconstructed perfectly. However, when different apertures are used for different samples—a common case in remote sensing—the deconvolution approach cannot be used. In the following we show how fixed or variable aperture functions can be incorporated into the reconstruction process to directly estimate the original signal.

2   One-Dimensional Sampling and Reconstruction

This section considers one-dimensional reconstruction. To simplify the development, we first consider uniform or regular sample reconstruction, then irregular sampling and reconstruction without an aperture function. Finally, the general case of irregular sampling with a variable aperture is considered.

2.1   Preliminaries

In discrete signal processing with periodic signals, the Dirichlet kernel plays an analogous role with the sinc function in continuous signal processing. The discrete Dirichlet kernel can be written as

$$D_{M,N}(n) \;=\; \sum_{k=-M}^{M} W_N^{-kn} \tag{4}$$

$$=\; \begin{cases} \dfrac{\sin((2M+1)\pi n/N)}{\sin(\pi n/N)}, & n \neq 0 \\ 2M+1, & \text{else} \end{cases} \tag{5}$$

which is periodic in n with period $N > 0$ and is M-band-limited. An illustrative plot of $D_{M,N}(n)$ for a particular M and N is shown in Fig. 1.

Since

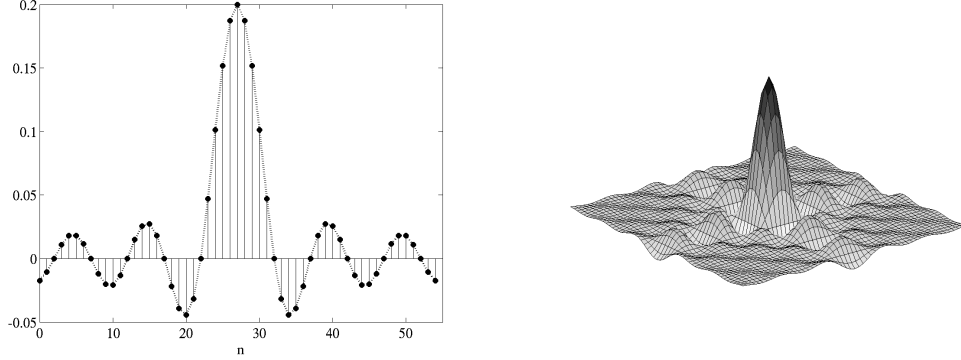$$\langle D_{M,N}(n - n_i), D_{M,N}(n - n_j) \rangle$$

Figure 1: Examples of (left) one-dimensional ($N = 55$, $M = 5$) and (right) two-dimensional ($N_1 = N_2 = 55$, $M_1 = M_2 = 5$) Dirichlet kernels. One period of each kernel is shown.

$$= \sum_{i=0}^{N-1} \sum_{j=0}^{N-1} D_{M,N}(n - n_i) D_{M,N}(n - n_j)$$
$$= N D_{M,N}(n_i - n_j), \tag{6}$$

it follows that $D_{M,N}(n - n_i)$ and $D_{M,N}(n - n_j)$ are orthogonal if and only if $(n_i - n_j)(2M + 1) = n'N$ for some integer $n' \neq 0$. The set of vectors generated by $D_{M,N}(n - jd); j = 0, 1, ..., 2M$ for integer $d = N/(2M + 1)$ forms an orthogonal basis for the space of all of discrete band limited functions of period N.[6] Thus, any discrete M-band-limited function with period N can be expressed as

$$f[n] \quad = \quad \sum_{j=0}^{2M} a_j D_{M,N}(n - jd) \tag{7}$$

with $f[n + kN] = f[n]$ for all integer k. This is the discrete equivalent of Eq. 1 when $a_j = \frac{d}{N} f[jd]$ and corresponds to interpolation by the Dirichlet kernel. Note that by construction $f[n]$ is M-band-limited and periodic with period N.

Equation 7 can be formulated as the matrix equation

$$\mathbf{f} = \mathbf{Da} \tag{8}$$

where the N element signal vector $\mathbf{f}$ has elements $(\mathbf{f})_n = f[n]$, $\mathbf{a}$ has $2M + 1$ elements a_j, and the $N \times (2M + 1)$ matrix $\mathbf{D}$ has elements

$$(\mathbf{D})_{k,l} = D_{M,N}(k - ld). \tag{9}$$

---

[6]Strictly speaking, d does not need to be an integer; however, when d is not an integer the a_j in Eq. 8 correspond to Dirichlet-interpolated values of $f[n]$ rather than to specific samples of $f[n]$. Nevertheless, the reconstruction equations [Eqs. 8, 11, and 12 for regular sampling, Eqs. 14 and 16 for irregular sampling] can be applied for non-integer d.

so that

$$D = \left[\ \mathbf{D}_{M,N}(0) \ \middle|\ \mathbf{D}_{M,N}(d) \ \middle|\ \cdots \ \middle|\ \mathbf{D}_{M,N}(2Md)\ \right]. \tag{10}$$

Equation 8 is the matrix formulation of the regular reconstruction equation. As shown later, this result can be generalized to deal with irregularly spaced sampling.

2.2 Reconstruction from Regular Samples

The regular, or uniform, discrete-time sampling and reconstruction problem can be formulated as follows. Any periodic, M-band-limited discrete signal f with period N, can be reconstructed exactly from $R \geq 2M + 1$ samples $f_s[j]$ where $f_s[j] = f[jd]$ with d is the integer sample spacing and $jd \bmod N$ distinct. Ideally, $R = N/d$.

The regularly sampled signal $f_s[n]$ can be written as,

$$\mathbf{f}_s = \mathbf{D}_\circ \mathbf{a} \tag{11}$$

where $\mathbf{D}_\circ$ is the $R \times (2M + 1)$ matrix constructed from the R rows of $\mathbf{D}$ corresponding to the values $n = jd;\ j = 0, 1, ..., R - 1$ with $\mathbf{f}_s$ containing $2M + 1$ elements $(\mathbf{f}_s)_k = f[kd]$.

Given $\mathbf{f}_s$, we want to compute $\mathbf{a}$. In order to compute the $2M + 1$ values in $\mathbf{a}$ necessary to fully reconstruct the signal, it is sufficient to show that the inverse of $\mathbf{D}_\circ$ exists. Then

$$\mathbf{a} = \mathbf{D}_\circ^{-1} \mathbf{f}_s. \tag{12}$$

$\mathbf{a}$ can then be used to reconstruct the signal using the reconstruction equation, Eq. 8.

For the regular sampling case with $R = 2M + 1$, the elements of the matrix $\mathbf{D}_\circ = \mathbf{D}$ can be written explicitly as

$$(\mathbf{D}_\circ)_{l,m} = D_{M,N}(ld - md) = \sum_{k=-M}^{M} W_N^{-kld} W_N^{kmd}. \tag{13}$$

As demonstrated in the appendix, the $\mathbf{D}_\circ$ matrix is always invertable so that Eq. 12 can be used to compute $\mathbf{a}$, which can then be used to reconstruct the signal using the discrete sampling equation $\mathbf{f} = \mathbf{D}\mathbf{a}$. We note that for the regular sampling reconstruction case with $d(2M + 1) = N$, $\mathbf{D}_\circ$ (d integer) is, in fact, a scaled identity matrix so that $\mathbf{a} = \frac{d}{N}\mathbf{f}_s$.

When the signal is oversampled, i.e. there are more than the minimum required $2M + 1$ signal samples available, the matrix $\mathbf{D}_\circ$ is rectangular but still has full column rank. In this case, the Moore-Penrose pseudoinverse can be used in place of the conventional inverse in Eq. 12, resulting in a unique estimate of $\mathbf{a}$. If there is no noise in the problem, the solution for $\mathbf{a}$ is precisely the same for all $N \geq R \geq (2M + 1)$. A longer discussion on oversampling is provided in the next section.

2.3 Reconstruction from Irregular Samples

The previous derivation can be extended to the case of sampling a signal at irregular intervals. The $R = 2M + 1$ irregular samples $\mathbf{f}_{is}$ can be represented in matrix form as

$$\mathbf{f}_{is} = \mathbf{D}_\Delta \mathbf{a} \tag{14}$$

where $\mathbf{D}_\Delta$ is the $R \times (2M+1)$ matrix constructed from the R rows of $\mathbf{D}$ corresponding to the distinct sample points $n_l \in \{0, ..., N-1\}$; $l = 1, 2, ..., R$ with $\mathbf{f}_{is}$ having the R elements $(\mathbf{f}_{is})_l = f[n_l]$. The elements of the matrix $\mathbf{D}_\Delta$ can be written explicitly as

$$
\begin{aligned}
(\mathbf{D}_\Delta)_{l,m} &= D_{M,N}(n_l - md) \\
&= \sum_{k=-M}^{M} W_N^{-kn_l} W_N^{kmd}.
\end{aligned}
\tag{15}
$$

In order to compute the $2M+1$ values of $\mathbf{a}$ necessary to fully reconstruct the signal [using Eq. 8], $\mathbf{D}_\Delta^{-1}$ must exist. This is shown in the appendix for arbitrary disjoint n_j.

While it is possible to write $\mathbf{D}_\Delta^{-1}$ in closed form, the closed-form inverse is impractical for numerical computation. Instead, well-known conventional numerical inverse methods can be used to compute $\mathbf{D}_\Delta^{-1}$ or solve the corresponding linear system. We point out that $\mathbf{D}_\Delta$ and $\mathbf{D}_\Delta^{-1}$ depend only on the sample locations and not the sample values. Thus, if the sample locations remain the same, multiple reconstructions can be accomplished with only one matrix inversion. Fast numerical methods for solving Eq. 14 are considered in [6].

Since $\mathbf{D}_\Delta^{-1}$ exists, it is possible (at least theoretically) to compute

$$
\mathbf{a} = \mathbf{D}_\Delta^{-1} \mathbf{f}_{is}
\tag{16}
$$

no matter what the precise values of the n_j are, so long as they are distinct. Once $\mathbf{a}$ is computed, it can then be used to reconstruct the signal using the discrete sampling equation, Eq. 8. Reconstruction from irregular samples can thus be viewed as a two-step process: first compute the frequency coefficients of the signal using Eq. 16, then reconstruct the full signal using Eq. 8.

We point out that once $\mathbf{a}$ is computed from the locations of the irregular samples, the reconstruction of $f[n]$ is independent of the original sample locations. Further, when there is no sampling noise, the $\mathbf{a}$ computed from either irregular or regular sampling is identical. Some computation can be saved if the reconstructed signal is only needed at particular locations. In this case $\mathbf{a}$ is first computed from the samples. Then the forward reconstruction equation, Eq. 8, can be used with $\mathbf{D}$ containing only the rows corresponding to the desired locations.

In the oversampled case where $R > 2M+1$, $\mathbf{D}_\Delta$ is rectangular but remains full column rank. It is overdetermined and therefore has a unique pseudoinverse. While the "extra" samples could be discarded to make $\mathbf{D}_\Delta$ square, retaining all of the samples improves the performance in the presence of sampling noise [6]. When $R > 2M+1$, the pseudoinverse is used in Eq. 16 to compute $\mathbf{a}$. We note that in the noise-free case, the same $\mathbf{a}$ results no matter the number (subject to $R \geq 2M+1$) or the locations of the samples so long as they are distinct.

2.4 Variable Apertures

The previous section showed that a one-dimensional, discrete, periodic, M-band-limited signal can be reconstructed from $2M+1$ arbitrary irregular samples. There is no restriction on where the sample points are located - only that they are distinct. This result has

been derived previously [8]. However, the variable aperture case has not been previously considered. In this section, we consider the variable aperture case.

As noted, in practice the observed signal is frequently filtered through an aperture or point-spread function prior to sampling. Such may arise due to the response function of an antenna, lens, or other signal processing. In general, the aperture may be different for each observation. While the effects of a single, fixed aperture function can be removed by deconvolution, handling variable apertures requires a more general approach.

Let $v_j[n]$ be the aperture corresponding to the jth observation. Effectively, v_j is the impulse response of the aperture. Typically, the aperture is window-like with a central peak centered at the sample location and has a finite length. The aperture is generally much shorter than the signal, and thus has a wider bandwidth of support. Define the jth aperture-filtered signal as $f_j[n] = v_j[n] * f[n]$. Note that $f_j[n]$ is band-limited to the minimum bandlimit of the signal $f[n]$ or aperture function $v_j[n]$.[7] The jth sampled observation is $g_j = f_j[n_j]$.

Assuming $v_j[n]$ is reasonably well-behaved, we can write,

$$f_j[n] = v_j[n] * f[n] = \sum_{k=0}^{N-1} f[k]v_j[n-k] \tag{17}$$

where v_j is treated as periodic modulo N so that the observation samples $g_j = f_j[n_j]$, are

$$g_j = \left(v_j[n] * f[n] \right)\Big|_{n=n_j} \tag{18}$$

$$= \sum_{k=0}^{N-1} f[k]v_j[n_j-k]. \tag{19}$$

Using Eq. 7 the sample g_j can be written as

$$g_j = \sum_{k=0}^{N-1}\sum_{l=0}^{2M} a_l D_{M,N}(k-ld)v_j[n_j-k] \tag{20}$$

$$= \sum_{l=0}^{2M} a_l H_j(n_j; l) \tag{21}$$

where $H_j(n_j; l)$ is defined as convolution of the Dirichlet kernel $D_{M,N}(n-ld)$ and the aperture function $v_j[n]$ sampled at n_j, i.e.,

$$H_j(n_j; l) = \left[v_j[n] * D_{M,N}(n-ld) \right]\Big|_{n_j}. \tag{22}$$

In matrix form, the variable aperture sampling equation is

$$\mathbf{g} = \mathbf{D}_v\mathbf{a} \tag{23}$$

---

[7]Here we assume that none of the apertures have frequency nulls in the signal bandwidth.

where $(\mathbf{g})_j = g_j[n_j]$ and $\mathbf{D}_v$ is the $R \times (2M+1)$ sampling matrix whose rows are $H_j(n_j;l)$ for $l = 0, ..., 2M$. Explicitly,

$$
\begin{aligned}
(\mathbf{D}_v)_{j,l} &= H_j(n_j;l) \\
&= \sum_{k=0}^{N-1} v_j[n_j - k] D_{M,N}(k - ld) &\quad (24) \\
&= \sum_{k=0}^{N-1} v_j[n_j - k] \sum_{m=-M}^{M} W_N^{-m(k-ld)} &\quad (25) \\
&= \sum_{k=0}^{N-1} v_j[n_j - k] \sum_{m=-M}^{M} W_N^{-mk} W_N^{mld}. &\quad (26)
\end{aligned}
$$

Given the sample values $\mathbf{g}$, the vector $\mathbf{a}$ can be computed by inverting Eq. 23, if the sampling matrix $\mathbf{D}_v$ is invertable.

The matrix $\mathbf{D}_v$ is invertable if only if the columns of $\mathbf{D}_v$ are linearly independent, which depends on the relationship of the aperture functions as shifted to the sampling location. In the ideal aperture case, $v_j[n] = \delta[n - n_j]$, so that $\mathbf{D}_v = \mathbf{D}_\Delta$. Fortunately most practical apertures tend to be well-behaved. These include finite-length window-like apertures centered at the (distinct) sample locations.[8] In these cases the matrix $\mathbf{D}_v$ is invertable. Notably, a fixed aperture $(v_j[n] = v[n - n_j])$, where $v[n]$ is well-behaved such as a window function, ensures invertability.

If $\mathbf{D}_v$ is full-column rank, the value of $\mathbf{a}$ computed from the variable aperture samples is unique and permits reconstruction of $f[n]$ using Eq. 8 for any set of distinct sample locations (subject to $R \geq 2M + 1$) and apertures. When extra samples are available, the pseudoinverse can be used. In the noise-free case the result is precisely the same values for $\mathbf{a}$ as when the minimum number of distinct samples is used.

2.5 Computational Considerations

In the previous sections it is shown that regardless of where the signal is sampled, the resulting $\mathbf{D}_\Delta$ matrix is invertable, enabling reconstruction of the periodic, band-limited signal $f[n]$ given any $2M + 1$ samples within the period. The samples could, in fact, be adjacent. However, the sample locations do affect the computation of the inverse of the $\mathbf{D}_\Delta$ or $\mathbf{D}_v$ matrices as quantified by the condition number of the matrices. The condition number κ is the ratio of the largest to smallest eigenvalues. A large condition number implies the inverse is sensitive to numerical computation errors. Thus, poor condition numbers can limit the practical implementation of the approach even though the matrix is known to be invertable. We note that the condition number is a function only of the sample locations and aperture function, and not of the signal values.

As we have seen, reconstruction of the sampled signal involves the solution of the linear system given by Eq. 14 for the case of no aperture (which is equivalent to an ideal δ function

---

[8]An example of a poorly behaved aperture is $v_j[n] = 1$ (i.e., a "rect" window spanning a signal period), which results in a non-invertable $\mathbf{D}_v$.

aperture) or Eq. 23 for the aperture-filtered case. This can be computationally taxing, particularly for large R. When using no aperture, the active weights conjugate gradient Toeplitz method (ACT algorithm) [6] is a computationally efficient method for solving the system for one-dimensional reconstruction from irregular samples. The ACT method can be extended to a single, fixed aperture by first reconstructing the aperture-filtered signal from the samples and then deconvolving the aperture function and signal. However, the ACT algorithm does not support variable apertures.

For the variable aperture case, a numerical approach must be used. Fortunately, numerical methods permit solutions of very large order even when the condition number is quite large. Values of R in of hundreds or more are practical and large values can be used with very high-precision computation. While there are so many variations that it is difficult to generalize the effects of the variable aperture, we have found that most practical apertures tend to regularize $\mathbf{D}_\Delta$, reducing the condition number relative to an ideal (δ function) aperture. Occasionally for particularly poor sampling distributions, the apertures can degrade the condition number compared to an ideal aperture. While poorly behaved apertures can produce non-invertable $\mathbf{D}_v$ matrices, in the authors' experience, poorly behaved apertures are rarely encountered in practice.

Iterative approaches to matrix inversion or linear system solution can be very effective for reconstruction, and iterative methods are commonly used to refine matrix inverses computed using QR factorization or other methods. We note that iterative methods can also be used to compute approximate reconstructions. These are particularly useful for very large problems with thousands or millions of samples. Examples of iterative reconstruction methods include algebraic reconstruction methods (e.g., [12]) and the scatterometer image reconstruction (SIR) method [13]. Though SIR was not originally explicitly formulated as a discrete reconstruction method, the linear form of SIR is an iterative approximation of the reconstruction method described here. Other variations are possible, e.g., [14].

3 Two-Dimensional Sampling and Reconstruction

Extending the one-dimensional results to higher dimensions seems straight-forward. However unlike in the one-dimensional case where the only requirements on the sample locations are that they be distinct, in the two-dimensional sampling case there are some sampling distributions that do not enable two-dimensional reconstruction. For example, if all the samples are in a straight line, they are effectively single-dimensional and general two-dimensional reconstruction is not possible.[9] On the other hand, for two-dimensional signals band-limited to rectangular spectrum of support, sampling using a generalized "cubic lattice" location scheme (defined later) is always fully reconstructable, even if the lattice spacing is nonuniform. While general two-dimensional sample location requirements that enable full reconstruction of band-limited signals are difficult to simply state, a given sampling configuration can be tested by evaluating the rank of the two-dimensional reconstruction matrix described later.

---

[9]Other examples of non-reconstructable sample distributions can be generated; see Fig. 2.
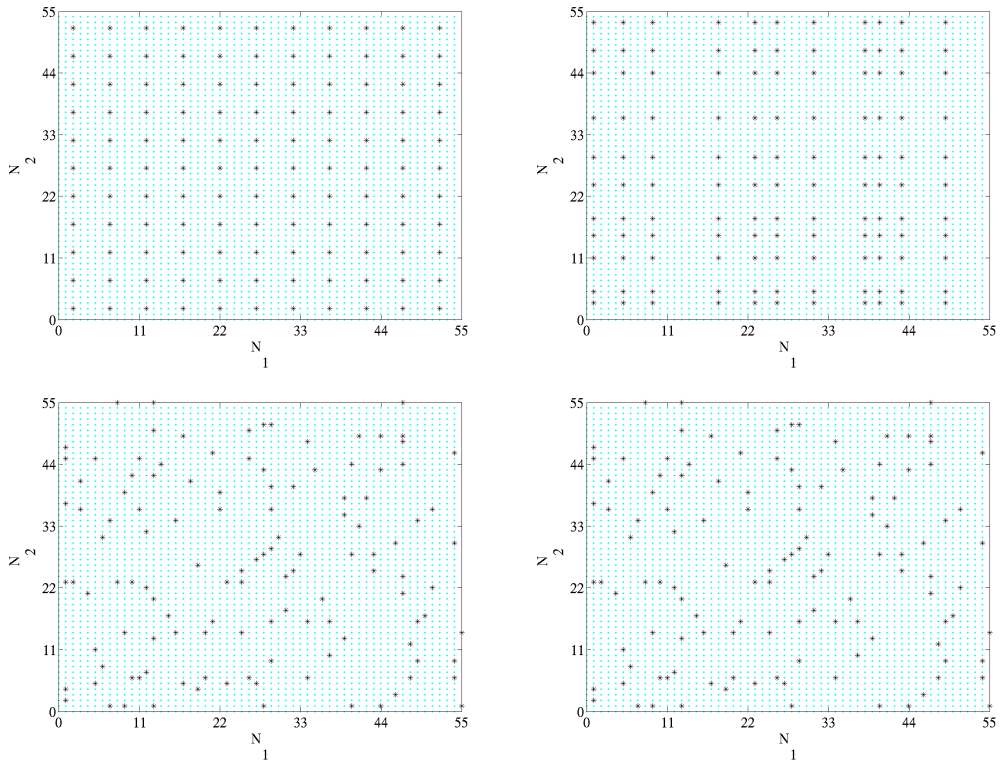
Figure 2: Examples of 2-D sampling for $(N_1 = N_2 = 45, M_1 = M_2 = 5)$: (ul) uniform cubic lattice; (ur) irregular cubic lattice; (ll) general reconstructable; (lr) non-reconstructable.

3.1   Preliminaries

Following the one-dimensional case, a discrete two-dimensional signal $f[n_1, n_2]$ with two-dimensional period $[N_1, N_2]$ is considered that is $[M_1, M_2]$-band-limited, i.e. the signal has a rectangular region of support in the frequency domain.[10] Thus, its two-dimensional DFT $F[k_1, k_2]$ can be written as (compare Eq. 3)

$$F[k_1, k_2] = \sum_{n_1=0}^{N_1-1} \sum_{n_2=0}^{N_2-1} f[n_1, n_2] W_{N_1}^{k_1 n_1} W_{N_2}^{k_2 n_2}. \tag{27}$$

Since $F[k_1, k_2]$ is $[N_1, N_2]$-periodic, we need only consider a single period in the following discussion.

For convenience the two-dimensional signal is expressed as a row-major ordered vector, though any consistent ordering could be used. Over a $[N_1, N_2]$ period, $f[n_1, n_2]$ is written in row-major ordering as the $N_1 N_2$ length vector $\mathbf{f}$ with elements $(\mathbf{f})_j = f[n_1, n_2]$ where $j = n_2 N_1 + n_1$ with $n_1 \in \{0, 1, \dots, N_1\}$ and $n_2 \in \{0, 1, \dots, N_2\}$. To illustrate the ordering, the two-dimensional locations

$$\begin{bmatrix} (0,0) & (0,1) & \cdots & (0, N_2-1) \\ (1,0) & (1,1) & \cdots & (1, N_2-1) \\ \vdots & \vdots & \ddots & \vdots \\ (N_1-1,0) & (N_1-1,1) & \cdots & (N_1-1, N_2-1) \end{bmatrix}$$

become the one-dimensional vector

$$\begin{bmatrix} (0,0) \\ (1,0) \\ (2,0) \\ \vdots \\ (N_1-1,0) \\ (0,1) \\ (1,1) \\ \vdots \\ (N_1-1,1) \\ (0),3 \\ (1,2) \\ \vdots \\ (N_1-1, N_2-1) \end{bmatrix}.$$

Eq. 27 defines a rectangular region of support in the frequency domain where $F[k_1, k_2] = 0$ for $|k_1| > M_1$ or $|k_2| > M_2$. Note that there are only R, where $R = R_1 R_2$ with $R_1 =$

---

[10]Other definitions of 2-D bandlimit exist that couple the coordinates. These have different sampling requirements [2, 15]. This report considers only a rectangular region of support to define the bandlimit.

$2M_1 + 1$ and $R_2 = 2M_2 + 1$, non-zero entries in $F[k_1, k_2]$. Thus, the minimum number of samples required to fully reconstruct an arbitrary $[M_1, M_2]$-band-limited signal is R.

In conventional sampling theory, the samples are required to be located on a regular (uniformly spaced) two-dimensional grid (known as a "uniform cubic lattice"), e.g., the $n_{i,j}^{th}$ sample is at $[id_1, jd_2]$ where $d_1 = N_1/(2M_1 + 1)$ and $d_2 = N_2/(2M_2 + 1)$ (d_1 and d_2 integer.)[11] Such a sampling is a specific example of the more general "generalized cubic lattice" sampling scheme defined as the cross product of two one-dimensional samplings, one along each dimension [15].

Consider R_1 distinct sample indexes $(n_1)_i \in \{0, ..., N_1 - 1\}$ and R_2 distinct indexes $(n_2)_j \in \{0, ..., N_2 - 1\}$. The sampling location sets $\{(n_1)_i\}$ and $\{(n_2)_j\}$ are termed the "marginal samplings". A gridded cubic lattice sampling consists of $R = R_1 R_2$ samples located at $n_{i,j} = [(n_1)_i, (n_2)_j]$.

In contrast to generalized cubic sampling, general two-dimensional sampling has R distinct samples arbitrarily located within a spatial period, with no structure required. Figure 2 illustrates examples of these different two-dimensional sampling schemes.

3.2   Two-dimensional Reconstruction

In this section it is shown that cubic lattice sampling can be a sufficient condition for full reconstruction; however, it is not a necessary condition for general $[M_1, M_2]$-band-limited reconstruction—many other general sampling configurations are possible. A method for evaluating these more general cases is derived. Unlike the one-dimensional case, merely having R disjoint samples is not sufficient to ensure full reconstruction—the sampling must be full-rank.

The condition expressed in Eq. 27 means that an arbitrary $[M_1, M_2]$-band-limited discrete two-dimensional signal $f[n, m]$ can be written as

$$f[n_1, n_2] = \sum_{p_1=0}^{2M_1} \sum_{p_2=0}^{2M_2} a_{p_1, p_2} D_{M_1, N_1}(n_1 - p_1 d_1)$$
$$D_{M_2, N_2}(n_2 - p_2 d_2), \tag{28}$$

which is the two-dimensional equivalent of Eq. 7 where the two-dimensional Dirichlet kernel is formed from product of two one-dimensional Dirichlet kernals, see Fig. 1.

In matrix-vector notation, the row-major ordered two-dimensional equivalent to Eq. 8 is

$$\mathbf{f} = \boldsymbol{\mathcal{D}}\mathbf{a} \tag{29}$$

where $\mathbf{a}$ is an $R = R_1 R_2$ vector with $(\mathbf{a})_l = a[p_1, p_2]$, $p = p_2 R_1 + p_1$ and $\boldsymbol{\mathcal{D}}$ is an $(N_1 N_2) \times R$ element matrix of sampled Dirichlet kernels where

$$(\boldsymbol{\mathcal{D}})_{k,l} = D_{M_1, N_1}(n_1 - p_1 d_1) D_{M_2, N_2}(n_2 - p_2 d_2) \tag{30}$$

---

[11] As in the one-dimensional case, non-integer d_1 and d_2 can be used; however, as in the one-dimensional case, for simplicity here we assume integer values for d_1 and d_2. Thus, N_1 and N_2 are integer multiples $2M_1 + 1$ and $2M_2 + 1$, respectively.

with $k = n_2 N_1 + n_1$ and $l = p_2 R_1 + p_1$. Thus, $\boldsymbol{\mathcal{D}}$ has a block form that can be constructed from two $\mathbf{D}$ matrices [Eq. 9] using the appropriate M and N values, e.g., $\boldsymbol{\mathcal{D}}$ can be expressed as the Kronecker or direct product of the $\mathbf{D}$ matrices along each axis, i.e.,

$$\boldsymbol{\mathcal{D}} = \mathbf{D}_{(1)} \otimes \mathbf{D}_{(2)} \tag{31}$$

where $\otimes$ is the Kronecker product[12] and $\mathbf{D}_{(1)}$ and $\mathbf{D}_{(2)}$ are $\mathbf{D}$ matrices constructed using M_1, N_1 and M_2, N_2, respectively. Recalling the one-dimensional development, we note that $\mathbf{a}$ corresponds to an equivalent uniformly spaced regular cubic lattice sampling of f, i.e., for integer d_1 and d_2, $\mathbf{a} = \frac{d_1 d_2}{N_1 N_2} \mathbf{f}_u$ where $(\mathbf{f}_u)_l = f[p_1 d_1, p_2 d_2]$.

Let $\{S_k\}$ be the set of $R_s \geq R$ distinct sample locations where $S_k = [(n_1)_k, (n_2)_k]$, with $0 \leq (n_1)_k < N_1$ and $0 \leq (n_2)_k < N_2$ arbitrary. The sampled signal vector $\mathbf{f}_s$ has elements $(\mathbf{f}_s)_k = f[S_k] = f[(n_1)_k, (n_2)_k]$ and can be written as

$$\mathbf{f}_s = \boldsymbol{\mathcal{D}}_\Delta \mathbf{a} \tag{32}$$

where the $R_s \times R$ matrix $\boldsymbol{\mathcal{D}}_\Delta$ consists of the appropriate rows of $\boldsymbol{\mathcal{D}}$, i.e., the kth row of $\boldsymbol{\mathcal{D}}_\Delta$ is the ith row of $\boldsymbol{\mathcal{D}}$ where $i = (n_1)_k N_2 + (n_2)_k$. Explicitly,

$$(\boldsymbol{\mathcal{D}}_\Delta)_{k,l} = (\boldsymbol{\mathcal{D}})_{i,l} = \tag{33}$$
$$D_{M_1, N_1}((n_1)_k - p_1 d_1) D_{M_2, N_2}((n_2)_k - p_2 d_2)$$

with $i = (n_2)_k N_1 + (n_1)_k$ and $l = p_2 R_1 + p_1$.

From Eq. 32 if $\boldsymbol{\mathcal{D}}_\Delta$ has full column rank (which at a minimum requires $R_s \geq R$), $\mathbf{a}$ can be uniquely computed from $\mathbf{f}_s$. We note that when $R_s > R$ and $\boldsymbol{\mathcal{D}}_\Delta$ is full column rank, some rows of $\boldsymbol{\mathcal{D}}_\Delta$ are linearly dependent on the other rows, which implies that excess rows and their corresponding samples can be eliminated (though extra samples are useful for noise suppression, see Sec. 3.4). We are often most interested in the case of critical sampling with $R_s = R$, which has square $\boldsymbol{\mathcal{D}}_\Delta$.

For cubic lattice sampling, it can be shown that

$$\boldsymbol{\mathcal{D}}_\Delta = \mathbf{D}_{\Delta(1)} \otimes \mathbf{D}_{\Delta(2)} \tag{34}$$

where $\mathbf{D}_{\Delta(1)}$ and $\mathbf{D}_{\Delta(2)}$ are one-dimensional forward sampling matrices defined in Eq. 15 for the marginal sampling sets $\{(n_1)_i\}$ and $\{(n_2)_j\}$. By using the well-known general matrix identity

$$\text{rank}(\mathbf{A} \otimes \mathbf{B}) = \text{rank}(\mathbf{A}) \, \text{rank}(\mathbf{B}), \tag{35}$$

where $\mathbf{A}$ and $\mathbf{B}$ are arbitrary matrices and noting that $\mathbf{D}_{\Delta(1)}$ and $\mathbf{D}_{\Delta(2)}$ are full column rank in Eq. 34, it follows that $\boldsymbol{\mathcal{D}}_\Delta$ is full rank. Thus for this case the marginal sampling

---

[12]The Kronecker product of a $m \times n$ matrix $\mathbf{A}$ and a $p \times q$ matrix $\mathbf{B}$ is a $mp \times nq$ matrix,

$$\mathbf{A} \otimes \mathbf{B} = \begin{bmatrix} a_{1,1}\mathbf{B} & \cdots & a_{1,n}\mathbf{B} \\ \vdots & \ddots & \vdots \\ a_{m,1}\mathbf{B} & \cdots & a_{m,n}\mathbf{B} \end{bmatrix}.$$

sets enable full reconstruction of arbitrary two-dimensional $[M_1, M_2]$-band-limited signals. This is true for either uniform or irregular marginal sampling schemes. For regular cubic lattice sampling with integer d_1 and d_2, $\mathcal{D}_\Delta$ is a scaled identity matrix and $\mathbf{a} = \frac{d_1 d_2}{N_1 N_2}\mathbf{f}_s$.

While $\mathcal{D}_\Delta$ is always full-rank for generalized cubic lattice sampling for more general sampling distributions, $\mathcal{D}_\Delta$ is not guaranteed to be full-rank, and in fact exceptions can be found. Despite extensive effort on our part, we have been unable to come up with simple description of the requirements for general sampling to ensure full-rank $\mathcal{D}_\Delta$; however, numerical methods can be used to test the rank of $\mathcal{D}_\Delta$ for any particular sampling to ensure invertability. This is discussed further in Sec. 3.4. Note that the rank of $\mathcal{D}_\Delta$ is dependent only on the sample locations and not on the sample values.

As in the one-dimensional case, reconstruction of the two-dimensional signal f from irregular samples can be viewed as a two-step process. First, the equivalent regular sampling representation $\mathbf{a}$ is computed from the irregular samples by solving Eq. 32, which is possible if $\mathcal{D}_\Delta$ is full-rank. The reconstructed signal is then computed using Eq. 29. Note that if the reconstructed signal is only needed at particular locations, $\mathbf{a}$ can be first computed. Then, f can be computed at the desired locations using the appropriate rows of $\mathcal{D}$ in Eq. 29, see Eq. 32.

3.3 Variable Apertures

As in the one-dimensional case, the effects of a single, constant aperture function for two dimensional sampling can be removed by deconvolution; however, a more general approach is required when different apertures are used with different samples.

Let $v_k[n_1, n_2]$ be the effective aperture corresponding to the kth observation. The sample value g_k is the two-dimensional convolution of the original signal and the aperture function, evaluated at the sample location, i.e.,

$$
\begin{aligned}
g_k &= \left. \Big(v_k[n_1, n_2] * f[n_1, n_2] \Big) \right|_{S_k} \\
&= \sum_{m_1}\sum_{m_2} f[m_1, m_2] v_k[(n_1)_k - m_1, (n_2)_k - m_2],
\end{aligned}
\tag{36}
$$

(compare Eqs. 18 and 19) where v_k is treated as periodic and the double sum is over the nonzero region of support for v_k and $S_k = [(n_1)_k, (n_2)_k]$ is the location of the aperture center. Let $\mathbf{g}$ be the R_s element vector of aperture-filtered samples. In matrix form, Eq. 36 is

$$
\mathbf{g} = \mathbf{D}_g \mathbf{f} = \mathcal{D}_g \mathcal{D}\mathbf{a} = \mathcal{D}_v \mathbf{a}
\tag{37}
$$

where the rows of $\mathcal{D}_g$ contain the values of v_k to be convolved with the columns of $\mathcal{D}$. The resulting rows of the $R_s \times R$ element matrix $\mathcal{D}_v$ are aperture-filtered Dirichlet kernels. Explicitly,

$$
\begin{aligned}
(\mathcal{D}_v)_{k,l} = \sum_{m_1}\sum_{m_2} v_k[(n_1)_k - m_1, (n_2)_k - m_2]\cdot \\
D_{M_1, N_1}(m_1 - p_1 d_1) D_{M_2, N_2}(m_2 - p_2 d_2),
\end{aligned}
\tag{38}
$$

$$= \sum_i \sum_j v_k[n_s - i, m_s - j] \cdot$$

$$\sum_{\mu_1=-M_1}^{M_1} \sum_{\mu_2=-M_2}^{M_2} W_{N_1}^{-\mu_1(i-pd_1)} W_{N_2}^{-\mu_2(j-qd_2)} \tag{39}$$

$$= \sum_{m_1} \sum_{m_2} v_k[(n_1)_k - m_1, (n_2)_k - m_2] \cdot$$

$$\sum_{\mu_1=-M_1}^{M_1} \sum_{\mu_2=-M_2}^{M_2} W_{N_1}^{\mu_1 m_1} W_{N_1}^{p_1 d_1} W_{N_2}^{-\mu_2 m_2} W_{N_2}^{p_2 d_2} \tag{40}$$

with $l = p_2 R_2 + p_1$.

By solving Eq. 37 with the sample values $\mathbf{g}$, $\mathbf{a}$ can be computed if the variable aperture sampling matrix $\boldsymbol{\mathcal{D}}_v$ is invertable. If $\boldsymbol{\mathcal{D}}_v$ is not invertable, then $\mathbf{a}$ cannot be precisely computed and so the signal cannot be exactly reconstructed from the samples. In this case approximate solution methods must be used, e.g., [9][13].

The matrix $\boldsymbol{\mathcal{D}}_v$ is invertable if only if it has full column rank, which depends on the relationship of the apertures as shifted to the sampling location. Including the apertures generally does not change the sampling rank. In numerical experiments described below we have found that the apertures often improve the condition number compared to the ideal-aperture matrix, i.e., they tend to regularize the sampling matrix. However, this is not always the case: some aperture functions and samplings do not result in a full-rank $\boldsymbol{\mathcal{D}}_v$. At present we do not have a general analytic method for specifying such cases and must rely on numerical tests. We hope to complete a more detailed exploration of the relationship between the variable apertures and the sampling locations in a future paper.

As in the one-dimensional case, reconstruction of the two-dimensional signal f from irregular variable aperture samples is a two-step process. Assuming $\boldsymbol{\mathcal{D}}_v$ is full-rank, the equivalent regular sampling representation $\mathbf{a}$ is first computed from the irregular samples by solving Eq. 37. The reconstructed signal is then computed using Eq. 29.

3.4   Two-dimensional Sampling Considerations

As previously noted, while cubic lattice sampling can ensure a full-sampling matrix in two-dimensional sampling, there is no guarantee that an arbitrary two-dimensional sampling is full-rank. To help provide insight into how often an arbitrary two-dimensional sampling does not result in a full-rank sampling matrix, we conduct a Monte Carlo experiment. For simplicity, we set $M = M_1 = M_2$ and $N = N_1 = N_2$. Two cases for the aperture function were considered: an ideal aperture (a δ function) and a realistic fixed aperture. The latter is a two-dimensional Hann window of extent M centered at the sample location. The experiment also evaluates the effect of "excess" samples when the number of samples R_s is greater than the minimum number R required for reconstruction.

While cases for small M and d can be reasonably exhaustively tested, this is not practical for larger values, so to generate this plot for each case and set of parameters, several thousand different realizations of sets of R_s distinct sample locations were randomly generated. The sample locations were uniformly distributed over the possible locations. For
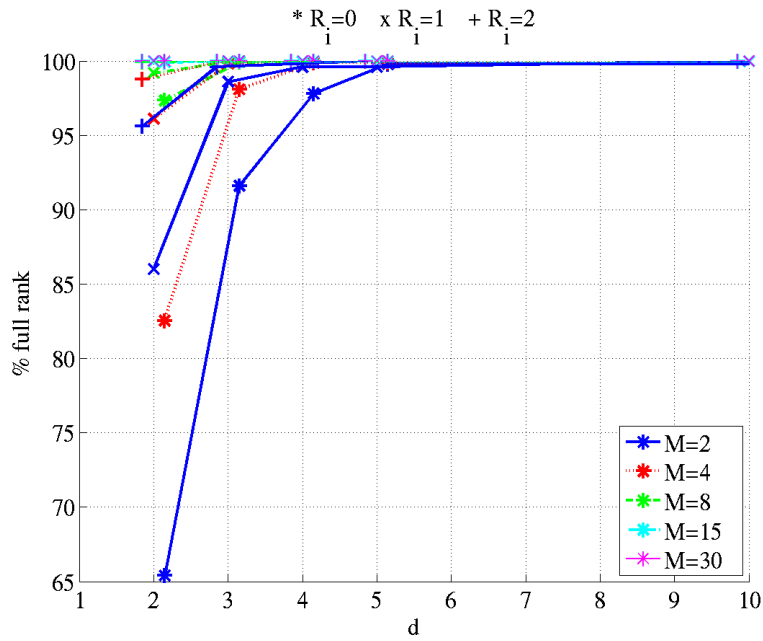
Figure 3: Numerically computed percentage of random 2D samplings that produce full-rank reconstruction matrices versus $d_1 = d_2 = d$ for different values of $M_1 = M_2 = M$. R_i indicates the number of additional samples above the minimum R required. In this figure, the line/symbol color is associated with M while different symbols indicate different R_i values. Lines and a small horizontal offset are added to the symbol locations to improve clarity.

each realization, the rank of the sampling matrix $\boldsymbol{\mathcal{D}}_v$ was numerically determined, and the percentage of full rank matrices computed. The results are summarized in Fig. 3.

In all cases this plot shows that the percentage of full-rank two-dimensional samplings for various values of M and d where $N = d(2M+1)$ increases with increasing M. The rate of increase is a function of d, with larger d producing higher full-rank matrix percentages. For $d > 6$ the percentage is almost always 100% for the M values considered. We observe that including the realistic aperture function improves the condition number of the sampling matrix, but did not affect the number of full-rank cases for the conditions considered.

When extra samples are available (i.e., $R_s > R$), in principle they are redundant and are not required for reconstruction if the sampling matrix is already full-rank; however, since most measurements have noise or intrinsic variability, the extra samples can be exploited to reduce the effects of noise by including them in the linear system solution when computing $\mathbf{a}$. This is equivalent to using a pseudoinverse.

In the full-rank case, the extra samples do not affect the signal reconstruction but tend to reduce the effects of sampling noise and improve the system condition number. However, when the sampling matrix is not full rank when $R_s = R$, including including extra samples (i.e., $R_s > R$) can result in a full-rank matrix. This is evident in Fig. 3 which compares different values of $R_\mathrm{i} = R_s - R$. Note that the percentage of full-rank cases increases with increasing R_i.

3.5   Sampling Noise

We briefly consider the effects of noise. From a reconstruction point of view, noise within the signal bandwidth included in the signal *prior* to sampling is treated as part of the signal. For such band-limited noise, the reconstruction does not affect the signal-to-noise ratio.

Noise (termed "sampling noise") added to the sample values as part of the sampling process or after sampling can affect the signal-to-noise ratio of the reconstructed signal. An example of sampling noise is the quantization error resulting from analog-to-digital conversion of the signal being sampled. Such quantization error is often modeled as independent additive noise with a white spectrum [16]. Another example of sampling noise arises in microwave remote sensing where the signal is a spatially dependent variable such as the surface brightness temperature or the normalized radar cross-section. When observed by a satellite sensor, the measurements are contaminated by thermal noise from the receiver [17] which has the effect of adding white noise to the measured value after spatial sampling by the antenna pattern and scanning geometry. Microwave sensors often use square-law detectors, which have the effect partially correlating the signal and noise and altering the noise probability distribution. For example, radiometer measurements have gamma- or chi-squared-like distributions [17].

For simplicity we consider only additive noise that is independent of the signal. The measurement noise equation is (see Eqs. 14 and 23)

$$\mathbf{f}'_s = \mathbf{f}_s + \eta_s = \boldsymbol{\mathcal{D}}_v \mathbf{a} + \eta_s \tag{41}$$

where $\mathbf{f}'_s$ is the vector of noisy observations of the signal samples $\mathbf{f}_s$ and η_s is the vector of

noise added to the signal samples. Typically, the elements of η_s are independent, identically-distributed (i.i.d.), though this is not required in the analysis that follows.

Given the noisy observations, the estimated sample vector $\hat{\mathbf{a}}$ is

$$\hat{\mathbf{a}} = \boldsymbol{\mathcal{D}}_\Delta^{-1}(\mathbf{f}'_s + \eta_s) = \mathbf{a} + \boldsymbol{\mathcal{D}}_\Delta^{-1}\eta_s = \mathbf{a} + \mathbf{a}_\eta \tag{42}$$

where $\mathbf{a}_\eta = \boldsymbol{\mathcal{D}}_\Delta^{-1}\eta_s$ is the noise with the inverse sampling filter applied. The reconstructed signal thus includes an additive term consisting of the noise filtered by the reconstruction matrix, i.e.

$$\hat{\mathbf{f}} = \boldsymbol{\mathcal{D}}\mathbf{a}' + \boldsymbol{\mathcal{D}}\mathbf{a}_\eta = \mathbf{f} + \eta_D \tag{43}$$

where $\eta_D = \boldsymbol{\mathcal{D}}\boldsymbol{\mathcal{D}}_\Delta^{-1}\eta_s$. Due to the filtering, the noise has different spectral and correlation properties in the reconstructed signal than it started with. The precise details depend on the sample locations and the aperture functions, as well as the noise properties. Some insight can be gained by examining the case of uniform sampling. For this case, the $\boldsymbol{\mathcal{D}}$ reconstruction matrix corresponds to an ideal low-pass filter and the added noise η_D term is the low-pass filtered noise values, i.e. the reconstruction matrix $\boldsymbol{\mathcal{D}}$ filters out frequency components of $\boldsymbol{\mathcal{D}}_\Delta^{-1}\eta_s$ that extend beyond the signal bandlimit. In the irregular sampling case, $\boldsymbol{\mathcal{D}}\boldsymbol{\mathcal{D}}_\Delta^{-1}$ is a more complicated filter that amplifies some components of the noise depending on the precise sampling and aperture functions.

For a particular sampling and set of aperture functions the post-reconstruction noise spectrum can be computed using standard spectral decomposition techniques via singular value decomposition of $\boldsymbol{\mathcal{D}}_\Delta$ [22]. Noise spectral components (eigenvectors) associated with small singular values of $\boldsymbol{\mathcal{D}}_\Delta$ are amplified, but any noise components outside of the signal bandlimit defined by $\boldsymbol{\mathcal{D}}$ are eliminated. As can be expected, we have found that oversampling tends to reduce noise amplification by reducing the span of the singular values.

4   Application Example

We now illustrate the application of the irregular reconstruction theory for a particular microwave sensor, considering both ideal and variable apertures. While the technique can be used for a variety of sensors, for this example we consider the passive microwave radiometer known as the Special Sensor Microwave/Imager (SSM/I) [18].

Capable of measuring up to seven different channels at different combinations of frequencies and polarization, the SSM/I is designed to measure radiometric emissions from the Earth [17]. Using a rotating antenna reflector and an integrate-and-dump filter, it collects a series of measurements over a wide swath. At the surface, the 3 dB antenna footprints range from about 15–70 km in the cross-scan direction and 13–43 km in the along-scan direction, depending on the beam and channel. We consider only a single beam. The measurement footprints have an elliptical shape whose size and aspect angle vary with measurement location in the swath [19].

Ignoring the effects of the atmosphere, an SSM/I measurement can be modeled as the integrated product of the surface brightness and the antenna pattern where the ith measurement z_i of the brightness temperatures is the time-average of the integral of the product

of the surface brightness response $T_b(x,y)$ and the spatial response function (the temporally integrated antenna gain pattern) $G_i(x,y)$ at the surface for the ith measurement [18]

$$z_i = \frac{1}{\overline{G_i}} \iint T_b(x,y) G_i(x,y) dxdy \qquad (44)$$

with

$$\overline{G_i} = \iint G_i(x,iy) dxdy. \qquad (45)$$

The spatial response function is thus the measurement aperture function.

Given the measurements z_i we want to estimate the surface brightness temperature T_b. To do this, following the discussion in Sec. I we assume T_b is band-limited, replace the integrals with summations of the sampled signals and aperture functions, and use reconstruction techniques to recover the band-limited T_b.

To illustrate the application of reconstruction theory, a simulation of the sampling and response function for the 37 GHz H-polarization SSM/I channel is conducted. A HSI pixel spacing[13] of 6.25 km is selected with the fine processing grid size set at $N_1 = N_2 = 100$, which corresponds to a 625 km × 625 km area. This is approximately one-half the nominal swath width, choosen for convenience.

Since the average spacing of the samples is approximately 25 km, we cannot expect the effective resolution of the reconstruction to provide much better resolution. Hence, we set $d_1 = d_2 = 4$ so that $M_1 = M_2 = 25$, which corresponds to 25 km signal resolution. Note that denser sampling (more samples over the same area) can support finer product image resolution. This can be achieved by combining multiple satellite passes over the target area [20].

The measurement response is modeled as an elliptical Gaussian function with one-half power dimensions of 37.5 km by 25 km. These are the measurement apertures. The ellipse aspect angle relative to the image grid is determined by the antenna scan angle, which varies across the swath. Figure 4a illustrates the measurement locations. Note that the measurements locations form an irregular sampling grid. Fig. 4b shows a few of the aperture functions which vary over the swath, resulting in spatially varying spatial response functions. The major axis of the aperture is aligned with the grid near the bottom, but is rotated by 60° near the top.

For the simulation a synthetic "truth" image is constructed at fine grid resolution as shown in Fig. 4d, that contains various features, including "spots" of varying sizes and image gradients. The span of T_b values is realistic for land imaging for the 37H SSM/I channel [19]. The truth image is ideally lowpass filtered to bandlimit it to 25 km resolution as shown in Fig. 4e. This image represents the best that can be recovered from the truth image in a $M_1 \times M_2$ band-limited sense. The mottling and feature smoothing in the image is the result of the ideal band limiting. The root-mean-square (RMS) difference between the band-limited and non-band-limited truth images is 4.80 K.

The various sampling and reconstruction matrices are numerically computed. The true $\mathbf{a}$ is computed using a two-dimensional fast Fourier transform (FFT). The $\boldsymbol{\mathcal{D}}$ matrix is

---

[13]The pixel spacing is the same as the 'posting resolution' or spacing of the reconstructed signal.
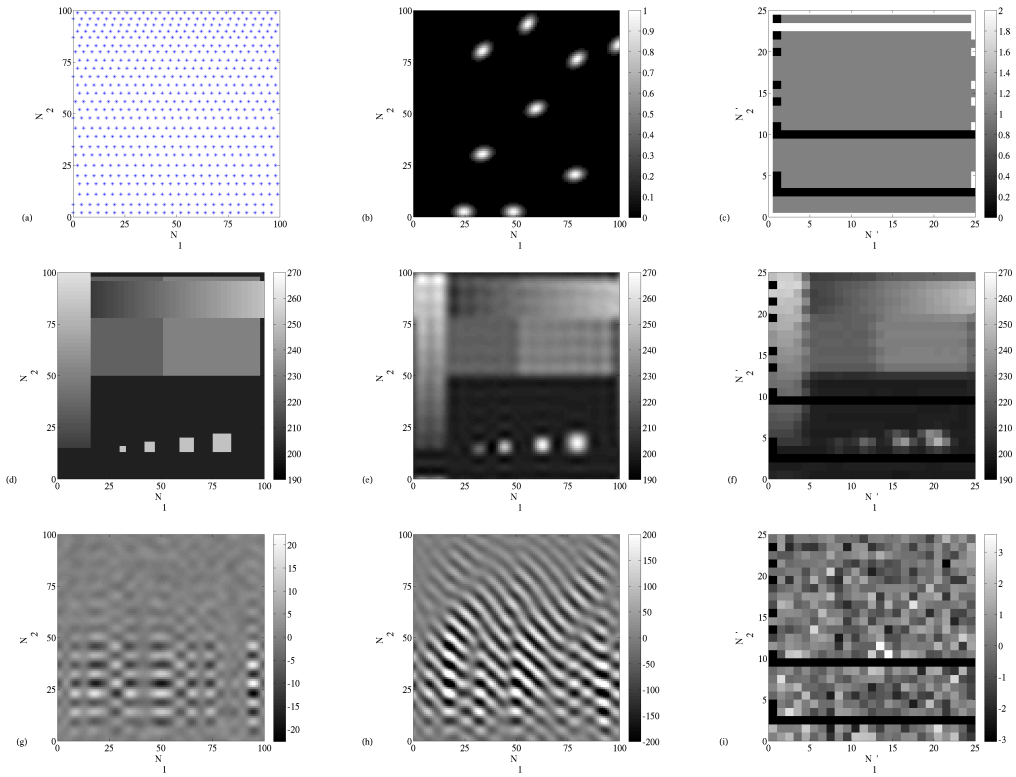
Figure 4: Illustrative results from an SSM/I measurement and reconstruction simulation. (a) Measurement locations. Underlying pixel spacing is 6.25 km. (b) Examples of the spatial measurement response function (aperture) at several locations. (c) Count of the number of measurements in each 25 km grid element. (d) Synthetic "truth" image (not band-limited). (e) Band-limited "truth" image. Bandlimit is at 25 km. (f) "Drop in the bucket" image. (g) Reconstructed noise without aperture. (h) Reconstructed noise with aperture. (i) "Drop in the bucket" noise example. Horizontal bands in lower portion of (c), (f), and (i) are DIB grid pixels containing no measurements–see text

Table 1: Summary of SSM/I simulation RMS difference statistics. The RMS difference between the band-limited and non-band-limited truth images is 4.80 K.

Case	Band-limited Truth	Non-band-limited Truth	Noise Term
Antenna Aperture	0.00	4.80	51.8
Ideal Aperture	0.00	4.80	2.65
Drop-in-the-Bucket	6.60	8.00	0.95

independent of the measurement locations and depends only on M_1, M_2, N_1, and N_2. Using the sampling locations in Fig. 4a, the $\boldsymbol{\mathcal{D}}_\Delta$ matrix is computed. The $\boldsymbol{\mathcal{D}}_v$ matrix is computed using the measurement-varying aperture function and and the measurement location. In this case there are $R = R_s = 625$ measurements. The $\boldsymbol{\mathcal{D}}_v$ matrix is full-rank.

Simulated noise-free measurements with ideal apertures are created along with simulated measurements for realistic spatially varying apertures using Eqs. 32 and 37, respectively. Noisy measurements are simulated by adding unit variance i.i.d. Gaussian noise to the simulated noise-free measurements.

Because $\boldsymbol{\mathcal{D}}_\Delta$ and $\boldsymbol{\mathcal{D}}_v$ are full-rank, the reconstruction from the noise-free measurements is exact to within numerical precision, i.e., both the ideal and realistic aperture reconstructions are the same as the true band-limited image in Fig. 4e. In these numerical experiments the condition numbers for the ideal and realistic aperture cases are 20 and 1982, which results in linear systems that are readily solvable with standard software.

Per Eq. 43 the noisy measurements are the sum of a noise term and the reconstructed signal. The noise terms for the same particular realization of the noise for the ideal and realistic apertures are shown in Figs. 4g and 4h. We observe that the unit variance additive noise has been significantly enhanced, particularly for the aperture case, where the reconstruction filter applied to the noise has created a diagonal ripple. It is thus apparent that for this particular problem, while the signal reconstruction is exact, the reconstruction of noisy measurements is sensitive to the noise level.

In conventional SSM/I data processing, the measurements are often gridded onto a 25 km grid $N_1' = N_2' = 25$ using a "drop-in-the-bucket" (DIB) technique where for each DIB grid element, all of the measurements whose centers fall within the grid element are averaged into the value reported by that pixel. The DIB resolution is limited to the sum of the grid size and the measurement response dimensions, in this case about 50 km or about twice as coarse as the reconstruction grid. The number of measurements falling within each DIB grid element is shown in Fig. 4c. Note that the number of measurements falling within a DIB grid element varies over the area and that some grid elements contain no measurements at all, resulting in gaps in the image, which are rows in this case. These gaps can be eliminated by increasing the grid size, which further lowers the image resolution. The DIB image estimate is shown in Fig. 4f. Note the reduced effective resolution of the DIB image compared to the reconstructed image, as well as the coarser features. Grid elements with no measurements are shown in dark blue. The DIB noise term is shown in Fig. 4i.

A comparison of the RMS errors for each image formation case is given in Table 1. Comparing the DIB, reconstructed images, and the RMS difference statistics, the improved accuracy and resolution of the reconstruction is apparent. However, the DIB noise level is also much smaller than the reconstructed case, so there is a tradeoff between resolution and noise level. This tradeoff can be exploited more finely using partial reconstruction techniques such as discussed in [13] and [20]. Whether a particular application can tolerate the higher noise level in exchange for finer effective resolution is application specific.

5 Conclusions

We have discussed the theory of signal reconstruction from irregularly sampled data with variable apertures where different measurements may have different aperture functions. This situation is common in microwave sensors where the observations have irregular spacing and different antenna gain patterns resulting in different measurement functions for different measurements.

The reconstruction methods presented in this report can be used for both real and complex signals. In either case the various D and $\mathcal{D}$ matrices are real.

We have focused on exact, band-limited reconstruction of a band-limited discrete signal. For the one-dimensional case, so long as there are a sufficient number of distinct samples and the aperture function is reasonably well-behaved, a band-limited periodic signal can be exactly reconstructed. In the two-dimensional case, the situation is more complicated, since not all sampling configurations can support full signal reconstruction. However, so long as the variable aperture function sampling matrix ($\mathbf{D}_v$ or $\boldsymbol{\mathcal{D}}_v$) is full column rank, a band-limited periodic function can be exactly reconstructed, within the limits of numerical precision, by inverting a linear system. When the samples have added noise, the sampling noise is filtered by the reconstruction matrix, which can enhance the impact of the noise. Example results are provided using a simulation based a realistic satellite sensor, the SSM/I microwave radiometer.

A number of illustrative numerical examples that demonstrate one- and two-dimensional irregular and variable aperture reconstruction are provided at `www.mers.byu.edu/reconstruction`. Matlab source code is included to illustrate the various reconstruction algorithms discussed.

We note that alternative reconstruction methods have been developed for the case when the signal is not band-limited or when only approximate or partially reconstructed results are needed, e.g., [2][3][4][12][13][20][21]. These may be numerically more efficient than the exact method considered here. Inexact methods that incorporate the noise statistics using Wiener-Kolmogorov smoothing to minimize the total error are also available, e.g., [22].

References

[1] A.V. Oppenheim and A.S. Willsky, *Signals and Systems*, Prentice Hall, Englewood Cliffs, NJ, 1983.

[2] M. Unser, "Sampling–50 years after Shannon," *Proc. IEEE*, vol. 88, no. 4, pp. 569–587, 2000.

[3] M. Migliaccio and F. Bruno, "A new interpolation kernel for SAR interferometric registration," *IEEE Trans. Geosci. Remote Sens.*, vol. 41, no. 5, pp. 1105–1110, 2011.

[4] M. Migliaccio, F. Nunziata, F. Bruno, and F. Casu, "Knab sampling window for InSAR data registration," *IEEE Trans. Geosci. Remote Sens. Lett.*, vol. 4, no. 3, pp. 397–400, 2011.

[5] H. Feichtinger and K. Gröchenig, "Iterative reconstruction of multivariate band-limited function from irregular sampling values," *SIAM Journal of Mathematical Analysis*, vol. 23, no. 1, pp. 244–261, 1992.

[6] H.G. Feichtinger, K. Gröchenig, and T. Strohmer, "Efficient numerical methods in non-uniform sampling theory," *Numerische Mathematick*, vol. 29, pp. 433–440, 1995

[7] K. Gröchenig, "Reconstruction algorithms in irregular sampling," *Mathematics of Computation*, vol. 59, no. 199, pp. 181–194, 1992.

[8] K. Gröchenig, "A discrete theory of irregular sampling," *Linear Algebra and Its Applications*, vol. 193, pp. 129–150, 1993.

[9] X. Xu, W. Ye, and A. Entezari, "Bandlimited reconstruction of multidimensional images from irregular samples," *IEEE Trans. Image Proc.*, vol. 22, no. 10, pp. 3950–3960, 2013.

[10] B.A. Williams and D.G. Long, "Reconstruction from aperture-filtered samples with application to scatterometer image reconstruction," *IEEE Trans. Geosci. Remote Sens.*, vol. 49, no. 5, pp. 1663–1676, 2011.

[11] W. Sun and X. Zhou, "Reconstruction of band-Limited signals from local averages," *IEEE Trans. Info. Theory*, vol. 48, no. 11, pp. 2955–2963, 2002.

[12] Y. Censor, "Finite series-expansion reconstruction methods," *Proc. IEEE*, vol. 71, no. 3, pp. 409-419, 1983.

[13] D.S. Early and D.G. Long, "Image reconstruction and enhanced resolution imaging from irregular samples," *IEEE Trans. Geosci. Remote Sens.*, vol. 39, no. 2, pp. 291–302, 2001.

[14] F. Lenti, F. Nunziata, C. Estatico, and M. Migliaccio, "On the spatial resolution enhancement of microwave radiometer data in Banach spaces," *IEEE Trans. Geosci. Remote Sens.*, vol. 52, no. 3, pp. 1834–1842, 2014.

[15] H.R. Künsch, E. Agrell, and F.A. Hamprecht, "Optimal Lattices for Sampling," *IEEE Trans. Info. Theory*, vol. 51, no. 2, pp. 634–647, 2005.

[16] A.V. Oppenheim and R.W. Schafer, *Discrete-Time Signal Processing*, Pearson Higher Education, Inc., Upper Saddle River, NJ, 2010.

[17] F.T. Ulaby and D.G. Long, *Microwave Radar and Radiometric Remote Sensing*, University of Michigan Press, Ann Arbor, MI, 2014.

[18] J.P. Hollinger, J.L. Pierce, and G.A. Poe, "SSM/I instrument evaluation," *IEEE Trans. Geosci. Remote Sens.*, vol. 28, pp. 781–790, Sep. 1990.

[19] D.G. Long and D.L. Daum, "Spatial resolution enhancement of SSM/I data," *IEEE Trans. Geosci. Remote Sens.*, vol. 36, no. 2, pp. 407–417, 1998.

[20] D.G. Long and M.J. Brodzik, "Optimum image formation for spaceborne microwave radiometers," submitted, *IEEE Trans. Geosci. Remote Sens.*, 2015.

[21] P.L. Butzer and J. Lei, "Approximation of signals using measured sampled values and error analysis," *Comm. App. Anal.*, vol. 4, pp. 245–255, 2000.

[22] M. Foster, "An application of the Wiener-Kolmogorov smoothing theory to matrix inversion," *J. Soc. Indust. Appl. Math.*, vol. 9, no. 3, pp. 387–392, 1961.

[23] M.E.A. El-Mikkawy, "Explicit inverse of a generalized Vandermonde matrix," *Applied Mathmematics and Computation*, vol. 146, pgs. 643–651, 2003.

A   Invertability of $\mathbf{D}_\circ$

For the regular sampling case with $R = 2M + 1$, the matrix $\mathbf{D}_\circ$ defined in Eq. 13 can be written as the product of two matrices, $\mathbf{D}_\circ = \mathbf{BC}$ where

$$
\mathbf{B} = \begin{bmatrix} W_N^{-Mn_0} & \cdots & W_N^{Mn_0} \\ \vdots & \ddots & \vdots \\ W_N^{-Mn_{2M}} & \cdots & W_N^{Mn_{2M}} \end{bmatrix} \tag{46}
$$

and

$$
\mathbf{C} = \begin{bmatrix} 1 & W_N^{Md} & \cdots & W_N^{M2Md} \\ \vdots & \vdots & \ddots & \vdots \\ 1 & W_N^{-Md} & \cdots & W_N^{-M2Md} \end{bmatrix}. \tag{47}
$$

Letting $W_N^{n_j} = b_j$; $j = 0, 1, ..., 2M$, then $W_N^{n_j l} = b_j^l$ and the matrix $\mathbf{B}$ can be written as

$$
\mathbf{B} = \begin{bmatrix} b_0^{-M} & \cdots & b_0^{-1} & 1 & b_0 & \cdots & b_0^M \\ \vdots & & \vdots & \vdots & \vdots & & \vdots \\ b_{2M}^{-M} & \cdots & b_{2M}^{-1} & 1 & b_{2M} & \cdots & b_{2M}^M \end{bmatrix}. \tag{48}
$$

We note that $\mathbf{B}$ is a Vandermonde matrix with complex entries b_i where $b_i \neq b_j \forall i \neq j$, $j = 0, 1, ..., 2M$. It is well-known that the inverse of a Vandermode matrix exists;[14] therefore $\mathbf{B}^{-1}$ exists.

Similarly, letting $W_N^{-(-M+k)d} = c_k$; $k = 0, 1, ..., 2M$, then $W_N^{-(-M+k)pd} = c_k^j$ and matrix $\mathbf{C}$ is

$$
\mathbf{C} = \begin{bmatrix} 1 & c_0 & c_0^2 & \cdots & c_0^{2M} \\ \vdots & \vdots & \vdots & & \vdots \\ 1 & c_{2M} & c_{2M}^2 & \cdots & c_{2M}^{2M} \end{bmatrix}, \tag{49}
$$

which is also a Vandermonde matrix with $c_i \neq c_j$ for $i \neq j$; therefore, $\mathbf{C}^{-1}$ always exists. Since $\mathbf{B}^{-1}$ and $\mathbf{C}^{-1}$ exist, and recalling that $\mathbf{D}_\circ = \mathbf{BC}$, it follows that $\mathbf{D}_\circ^{-1} = \mathbf{C}^{-1}\mathbf{B}^{-1}$ exists.

B   Invertability of $\mathbf{D}_\Delta$

The matrix $\mathbf{D}_\Delta$ defined in Eq. 15 can be factored as the product of two matrices $\mathbf{D}_\Delta = \mathbf{BC}$ where

$$
\mathbf{B} = \begin{bmatrix} W_N^{-Mn_1} & \cdots & W_N^{Mn_1} \\ \vdots & \ddots & \vdots \\ W_N^{-Mn_R} & \cdots & W_N^{Mn_R} \end{bmatrix} \tag{50}
$$

---

[14]In fact, a closed-form analytic inverse of a general Vandermode matrix has been developed [23].

and $\mathbf{C}$ is precisely the same matrix as in the regular case [Eq. 49]. Note that $\mathbf{C}$ is not dependent on the n_j values. Using $b_j = W_N^{n_j-1}$, $\mathbf{B}$ can be written as

$$\mathbf{B} = \begin{bmatrix} b_0^{-M} & \cdots & b_0^{-1} & 1 & b_0 & \cdots & b_0^M \\ \vdots & & \vdots & \vdots & \vdots & & \vdots \\ b_{2M}^{-M} & \cdots & b_{2M}^{-1} & 1 & b_{2M} & \cdots & b_{2M}^M \end{bmatrix}. \tag{51}$$

To see that $\mathbf{B}$ is invertable for any disjoint set of n_j values, note that the matrix $\mathbf{B}$ can be factored into the product of two matrices $\mathbf{B} = \mathbf{AV}$ where

$$\mathbf{A} = \begin{bmatrix} W_N^{-Mn_0} & 0 & 0 \\ \vdots & \ddots & \vdots \\ 0 & 0 & W_N^{Mn_0} \end{bmatrix} \tag{52}$$

and

$$\mathbf{V} = \begin{bmatrix} 1 & W_N^{n_0} & \cdots & W_N^{2Mn_0} \\ \vdots & \vdots & \ddots & \vdots \\ 1 & W_N^{n_{2M}} & \cdots & W_N^{2Mn_{2M}} \end{bmatrix}. \tag{53}$$

$\mathbf{A}$ is a diagonal matrix with nonzero diagonal elements, therefore $\mathbf{A}^{-1}$ exists. Letting $v_k = W_N^{n_k-1}$, $\mathbf{V}$ can be written as

$$\mathbf{V} = \begin{bmatrix} 1 & v_0 & v_0^2 & \cdots & v_0^{2M} \\ \vdots & \vdots & \vdots & & \vdots \\ 1 & v_{2M} & v_{2M}^2 & \cdots & v_{2M}^{2M} \end{bmatrix}, \tag{54}$$

which is a Vandermonde matrix with $v_i \neq v_j \forall i \neq j$; therefore, $\mathbf{V}^{-1}$ exists. Given that $\mathbf{A}^{-1}$, $\mathbf{V}^{-1}$, and $\mathbf{C}^{-1}$ exist and $\mathbf{D}_\Delta = \mathbf{BC} = \mathbf{AVC}$, it follows that $\mathbf{D}_\Delta^{-1} = \mathbf{C}^{-1}\mathbf{V}^{-1}\mathbf{A}^{-1}$ exists for any disjoint set of n_j.